MNRAS **000**, 1–14 (2016) Preprint 19 July 2016 Compiled using MNRAS LATEX style file v3.0

SWIFT view of the 2015 outburst of GS 2023+338 (V404 Cyg): complex evolution of spectral and temporal characteristics

Radhika D.,[1⋆] Nandi A.,[2] Agrawal V. K.[2] and Mandal S.[3]
[1] *Department of Physics, University of Calicut, Malappuram (District), 673635, India*
[2] *Space Astronomy Group, ISRO Satellite Centre, ISITE, Outer Ring Road, Near Karthik Nagar, Marathahalli, Bangalore, 560037, India*
[3] *Indian Institute of Space science and Technology, Trivandrum, 695547, India*

arXiv:1601.03234v2 [astro-ph.HE] 17 Jul 2016

Accepted XXX. Received YYY; in original form ZZZ

ABSTRACT

We study the spectral and temporal characteristics of the source GS 2023+338 (V404 Cyg) during the initial phase of its June 2015 outburst, over the energy range of 0.5 - 150 keV. This is the first detailed study of the characteristics of this source based on *SWIFT* observations, being reported. Based on our analysis, we understand that the source existed in the hard, intermediate and soft spectral states. We find that the evolution of the spectral parameters, the hardness intensity diagram and the rms-intensity diagram are not similar to those observed for most of the outbursting black hole sources. We also observe presence of weak peaked components in the power density spectra during the intermediate state of the source. Dramatic changes in the spectral and temporal properties are also exhibited before the ejection of a radio jet suggesting it to be associated with the coronal mass ejection. It seems that may be due to evacuation of the inner part of the Keplerian disc for a short duration, the disc component is not observed after the huge radio flare. The absorption features observed in the low energy spectra suggest the presence of wind emission and the evolution of the characteristics of the variable Fe line emission during both hard and intermediate states, indicate its origin to be probably related to the wind/outflow.

Key words: accretion, accretion discs – black hole physics – X-rays: binaries – ISM: jets and outflows – line: profiles – stars: individual: V404 Cygni

1 INTRODUCTION

Black hole transients have been observed to depict variability in spectral and temporal characteristics during their outbursts. The light curves for the outbursts of these sources are observed to be typically of fast rise and exponential decay (FRED) profile (e.g. XTE J1859+226 (Brocksopp et al. 2002), 4U 1543−47 (Park et al. 2004)), but a few sources are observed to show deviations from this (e.g. GRO J1655−40 (Kuulkers et al. 1998), GX 339−4 (Belloni et al. 2005)). The thermal emission from the Keplerian accretion disc around these objects contributes to the soft spectra (Shakura & Sunyaev 1973). The high energy spectra are resultant of the Comptonization of the seed photons from the disc by the hot electrons in the corona which may be static (Tanaka & Lewin 1995) in nature or a dynamical corona (Chakrabarti & Titarchuk 1995) that satisfactorily explains the spectral evolution observed in the outbursting black hole sources. The resultant high energy spectra, can some times have a cut-off at higher energies corresponding to the recoiling of the electrons.

The variation in contribution from different spectral components can give rise to spectral and temporal variabilities and based on these observed characteristics, black hole transients undergo spectral state transitions in their Hardness Intensity Diagram (HID) which typically has a 'q-shape' for most of the sources (Belloni et al. 2005; Dunn et al. 2010; Corral-Santana et al. 2016 and references therein). Remillard & McClintock 2006 classified these states into soft (HSS), hard (LHS) and very high states, while Belloni et al. 2005; Motta et al. 2012 and references therein further classified the very high state into hard-intermediate (HIMS) and soft-intermediate (SIMS) states with more emphasis on the timing properties of the sources (eg. types of QPOs, fractional rms variability etc.). With reference to these understandings of the combined spectral and temporal properties,

⋆ E-mail:radhikad_isac@yahoo.in

© 2016 The Authors

Debnath et al. 2008; Nandi et al. 2012; Radhika & Nandi 2014 have studied the evolution of spectral states in HID for several sources. The underlying principle of classification of states was purely based on the prescription of two component advective flow (Chakrabarti & Titarchuk 1995) model (see section 4 for details). Recently, this classification scheme is further corroborated based on the physical basis of accretion dynamics around several black hole sources (Debnath et al. 2015a,b; Iyer et al. 2015; Molla et al. 2016 and references therein).

In outbursting black hole sources the variation of source intensity with respect to the fractional rms variability is observed to show a hysteresis (Munoz-Darias et al. 2011; Kylafis & Belloni 2015) which is called as the rms-luminosity diagram (RLD). It has also been understood that a steady/compact jet exists during the LHS and HIMS (Fender et al. 2004, 2009 and references therein), while usually a transient relativistic jet is observed during the transition from HIMS to SIMS. Jets are not observed during the HSS. Hence, the characteristics of the source during the jet ejections help in understanding of the phenomenon of accretion-ejection or disc-jet coupling. The spectral and temporal characteristics of most of the outbursting black hole binaries, have been understood based on the continuous observations by Rossi X-ray Timing Explorer (RXTE) (Belloni et al. 2005; Remillard & McClintock 2006; Nandi et al. 2012).

The source GS 2023+338 is a black hole transient with a low mass optical companion V404 Cyg. It was discovered by the Ginga satellite during its outburst in 1989 (Makino 1989), and is located at an R.A. of 306.01° and DEC of 33.86°. The dynamical mass and distance of the source are estimated to be of $\sim 12 M_{\odot}$ (Shahbaz et al. 1994), and 2.39 $\pm$ 0.14 kpc (Miller-Jones et al. 2009), respectively.

The source has been observed to show variabilities in its light curve, by undergoing multiple flaring activity. The light curve of the source has been modeled as a triangular profile during its 1989 outburst (Kitamoto et al. 1989). The X-ray spectral and temporal characteristics of this source have been studied based on GINGA (Kitamoto et al. 1989) and ROENTGEN observations (in 't Zand et al. 1992; Oosterbroek et al. 1997), highlighting the changes in spectral index, variable low energy absorption and slight variations in the power spectrum with respect to typical black hole sources. The radio and X-ray correlation for the source during its 1989 outburst and quiescence phase has been performed by Corbel et al. 2008, and they observed the linear correlation to be consistent during the hard state of the source in its 1989 outburst and also later at the quiescence.

A recent outburst of V404 Cyg was detected by SWIFT-Burst Alert Telescope (BAT) on 15th June 2015 (i.e. MJD 57188), with follow-up observations by SWIFT-X-ray Telescope (XRT) (Barthelmy et al. 2015), Monitor of All-sky X-ray Image (MAXI) (Negoro et al. 2015), INTErnational Gamma-Ray Astrophysics Laboratory (INTEGRAL) (Kuulkers et al. 2015) and FERMI Gamma-ray Space Telescope (hereafter FERMI) (Younes 2015). Multi-wavelength observations were performed in Optical (Gazeas et al. 2015) and Radio (Mooley et al. 2015a; Trushkin et al. 2015b). In contrary to most of the black hole transients having typically one X-ray flare, for the source V404 Cyg multiple X-ray flares are observed during the 2015 outburst similar to its 1989 outburst (Ferrigno et al. 2015). The source achieves a peak X-ray flux approximately 10 days after the beginning of the outburst and later decays to the quiescence phase (Sivakoff et al. 2015). Detailed study of the spectral characteristics observed by INTEGRAL has been discussed by Rodriguez et al. 2015; Natalucci et al. 2015; Roques et al. 2015. They classified the spectral states into hard 'on-flare' and hard 'off-flare' states (i.e. hard spectra when a flare occurs and does not, respectively), and also obtained the seed photon temperature required for Comptonization to be >7 keV. Analysis of the FERMI-Gamma ray Burst Monitor (GBM) observations by Jenke et al. 2016 also suggested the source spectrum to be hard during the initial days of the outburst. Although the nature of the hard X-ray spectrum was understood by these studies, a detailed study of the contribution from the soft/thermal disc emission was not reported. Based on the INTEGRAL observations, the X-ray variability observed was attributed to the accreting source and also to the variable absorption by matter in the line of sight which was seen during the 1989 outburst too (in 't Zand et al. 1992). The Chandra-HETG observations have revealed the detection of emission lines in the spectrum of the source during the 2015 outburst, indicating strong disc wind emission (King et al. 2015).

Previous studies on this source based on the 1989 outburst, found that the source exhibited only a hard spectrum without any signature of the Keplerian disc. The timing analysis implied that the power density spectrum had flat-top noise similar to that observed during the hard states of black hole binaries. The spectral and temporal characteristics of the source were then correlated to the black hole source Cyg X−1 (in 't Zand et al. 1992; Oosterbroek et al. 1997). The INTEGRAL (Roques et al. 2015 and references therein) and FERMI (Jenke et al. 2016) observations of the 2015 outburst could classify the source into a hard state only.

In this paper, we consider SWIFT XRT and BAT observations of GS 2023+338 (V404 Cyg) during the initial phase of its 2015 outburst, so as to understand the spectral and temporal characteristics of the source when multiple X-ray and radio flares are observed. We consider the energy range of 0.5 - 150 keV, so as to look into the possible contributions of both the soft and hard emissions from the source. This paper for the first time gives a detailed analysis of the SWIFT XRT and BAT observations for the 2015 outburst of V404 Cyg. Although the SWIFT observations are not continuous unlike RXTE observations of outbursting sources[1], these are good enough to give an overall understanding of the evolution of the source characteristics, spectral states and HID. The previous outburst of this source has not exhibited any spectral state transition. We attempt to understand if any state transition takes place during the 2015 outburst. This is investigated by studying the variations of flux from the soft and hard components, hardness ratio and the fractional rms variability observed by both XRT and BAT. We attempt to understand the evolution of the Fe-line emission, and pres-

[1] V404 Cyg has not been observed by RXTE, but in this paper we discuss the spectral and temporal characteristics of the source based on the general understanding about black hole binaries that we have learned using RXTE observations.

ence of any absorption features during this outburst. We also explore the possible correlation between the X-ray characteristics and reported radio emissions.

A summary of the procedures followed for data reduction and analysis has been given in section 2. The results obtained from the spectral and temporal analysis are presented in section 3 and the same are discussed in section 4.

2 OBSERVATIONS, DATA REDUCTION AND ANALYSIS

We have analyzed the public archival data of the SWIFT satellite, available through the HEASARC database. Data are obtained for 23 observations beginning from MJD 55188 (15th June 2015) and up-to MJD 55201.99 (28th June 2015) when on-wards the dust scattering rings are observed (Beardmore et al. 2015; Vasilopoulos & Petropoulou 2016). Amongst these, simultaneous XRT and BAT observations exist for eight observations (i.e. MJD 57191.03, 57191.54, 57194.60, 57196.34, 57198.01, 57199.52, 57199.99 and 57200.92), four (i.e. MJD 57188.77, 57193.55, 57197.20 and 57198.15) have only BAT observations while the rest have only XRT. An observation log has been tabulated as part of the appendix. In this paper, we refer MJD 57188 as day 0, and all the other observations follow accordingly. The standard ftools provided by HEASOFT v 6.17 are used for the purpose of data reduction and analysis.

2.1 XRT data reduction

The SWIFT X-ray telescope (XRT) is a Wolter-type 1 telescope with a CCD at its focus and covers an energy range of 0.2 - 10 keV (Burrows et al. 2005). Amongst the different read-out modes of XRT, for the source V404 Cyg the observations are performed in the windowed-timing mode.

We obtain the cleaned XRT event products through the *xrtpipeline*. Using XSELECT v 2.4, events are generated corresponding to grades of *0-2* which consist of the valid X-ray events. For events without pile-up, a circle of radius 30 pixels is chosen for the source region. Since the source has been bright at a few intervals, the pile-up corrections are performed for these particular observations by selecting events from grades of only *0*. In this case, an annular region is chosen around the source centre. The outer radius of the annular is fixed at 30 pixels and the inner radius is selected by varying the number of pixels, based on the ratio of counts in grade 0 events to grade 0-2 events. An annular background region is considered far away from the source, referring to the standard methods for windowed-timing mode data. For the observations where the source has been contaminated by dust scattering, the background region is selected in such a way that it will subtract the contribution from the dust (A. Beardmore, 2015 private communication).

Since the extraction regions are not always similar, a scaling factor has been applied to the source and background spectral files, by editing the BACKSCAL keyword [2]. If the source region is circular with radius r_s, then a scaling factor of $2\times r_s$ is applied to the source spectra. The annular region chosen for the background has inner radius r_1 and outer radius of r_2, so the scaling factor applied is $r_2 - r_1$. The pixels at the end-of-window will be considered as bad by the ground software processing, thereby converting the image from 2-dimensional to 1-dimensional. The BACKSCAL keyword takes into account these and corrects the spectral information.

Uncertainty in position of the source has been taken care of, by applying the position dependent *rmfs* for the respective grades (see also Iyer et al. 2015). Those observations where the source is not piled-up, the rmfs used do not have these corrections [3]. The ftool *xrtmkarf* has been used along-with the exposure map, to generate the arf files for each observation. The source spectral data are re-binned to 25 counts per bin, by means of *grppha*.

Timing analysis of XRT data is performed by generating source and background light curves for the minimum time bin resolution of 1.8 ms, for the selected source and background regions. From these, we generate background subtracted light curves and use for further analysis.

2.2 BAT data reduction

The Burst Alert Telescope (BAT), has a large area solid state (i.e. CdZnTe) detector with energy range coverage of 15 - 150 keV and a large field of view (Krimm et al. 2013). The instrument is a very good monitor for the bursting sources (say GRBs, transients etc.), and also has good capabilities to study the spectral and temporal variabilities from a source.

The standard procedures for data reduction mentioned in the data analysis threads [4], have been employed to generate BAT spectra and light curves. We consider the event data for the analysis, referring to the analysis procedures provided in the BAT threads. Since the gain correction has already been applied in the BAT event file, we did not repeat the energy calibration [5]. Detector plane images (dpi) are generated for the energy range of 15 - 150 keV using *batbinevt*. The *batdetmask* is used to obtain the appropriate detector quality map with the help of the detector enable/disable map. Making use of these, the noisy detectors are found with the help of the ftool *bathotpix*, and a quality map is obtained as a result. Appropriate mask weighting is applied to the event data using *batmaskwtevt*. We generate energy spectra for the range of 15 - 150 keV by incorporating the quality map. Systematic errors are applied using *batphasyserr* to account for the residuals in the response, the ray-tracing keywords are corrected by *batupdatephakw*. Response matrix corresponding to the spectral file has been generated using *batdrmgen*.

BAT light curves are generated for a time bin of 0.01 sec over the energy range of 15 - 150 keV, with the help of the ftool *batbinevt*.

[2] http://www.swift.ac.uk/analysis/xrt/backscal.php

[3] http://www.swift.ac.uk/analysis/xrt/rmfs.php

[4] http://www.swift.ac.uk/analysis/bat/

[5] http://swift.gsfc.nasa.gov/analysis/threads/bateconvertthread.html

2.3 Analysis

Spectral analysis package of XSpec v 12.9 (Arnaud 1996) is used to perform simultaneous spectral analysis of the XRT and BAT data over an energy range of 0.5 - 150 keV, which we find to be the optimum energy range having statistically significant photon counts required for spectral fitting. Spectral modeling has been performed with the help of the *diskbb* (Mitsuda et al. 1984; Makishima et al. 1986), *compTT* (Titarchuk 1994) or *pexrav* (Magdziarz & Zdziarski 1995), *gauss*, *pcfabs* and *gabs* models.

The *diskbb* is used to model the low-energy photon emission from different radii of the Keplerian accretion disc. This model provides an estimate of the temperature at each radius of the disc (hence, a multi-coloured disc with blackbody spectra) and the contribution to the flux emitted in soft energy. The high energy spectrum will be a powerlaw which is occurring due to Comptonization of the soft photons by the corona. The *compTT* model describes the Comptonization process of relativistic thermal plasma. The *pexrav* considers a powerlaw spectrum with exponential cut-off, which gets reflected from a neutral material. We study the evolution of the photon index of the spectra, the reflection factor and the cut-off energy in order to understand the characteristics of the hard emission. Detailed information about the different models used in this paper can be obtained from the corresponding references and also in the XSpec manual.

The *gauss* model is used to study the fluorescent Fe-line emission signature in the spectrum, and the absorption features of the spectra are modeled by *pcfabs* and/or *gabs* (see section 3 and §4). The interstellar absorption has been considered using the *wabs* model (Wilms et al. 2000), and the hydrogen column density (n_H factor) is found to be varying between 0.6×10^{22} atoms cm^{-2} and 1.2×10^{22} atoms cm^{-2}, during the outburst.

The *cflux* model is used to obtain the source X-ray flux (i.e. unabsorbed flux) in the energy ranges 0.5 - 10 keV and 15 - 150 keV. The contribution of disc flux is estimated in 0.5 - 10 keV and that of the hard/powerlaw flux in 0.5 - 10 keV and/or 15 - 150 keV. We estimate the hardness ratio in XRT and BAT, by calculating the ratio of fluxes in 4 - 10 keV and 0.5 - 4 keV, 50 - 150 keV and 15 - 50 keV, respectively. Error bars for the different spectral parameters are obtained at 90% confidence interval, using the command *err*.

Timing analysis has been performed using the package XRONOS v 5.22. The frequency range considered is 0.068 Hz to 277.8 Hz for the XRT data of 1.8 ms time resolution and interval length of 8192 bins, and 0.012 Hz to 50 Hz for BAT data of time resolution 0.01 sec and interval length of 8192 bins. In order to search for the presence of QPOs, power density spectra (PDS) are generated for the same frequency range, using the ftool *powspec* v 1.0 by performing Fourier transform on the background subtracted lightcurves. The fractional rms variability is estimated by calculating the square root of the integrated power in the XRT lightcurve for the frequency range of 0.1 - 20 Hz, thereby neglecting the noise dominant frequency range. We calculate the error in rms variability at 90% confidence interval, by means of error propagation. Since BAT PDS has broad-band noise with less power, we did not estimate the rms variability for the same. We generate the XRT PDS with interval length of 65536 bins, resulting the frequency range to begin from 0.008 Hz, so as to search for mHz QPOs.

The Radio data have been obtained by Radio Astronomical Telescope of the Academy of Sciences (RATAN)-600, and we refer to the radio light curve provided by them (Trushkin et al. 2015b). Radio flaring has also been reported by Mooley et al. 2015a,b based on Arcminute Microkelvin Imager - Large Array (AMI-LA) observations at 16 GHz, Tsubono et al. 2015 using Waseda University Nasu radio telescope at 1.4 GHz and Tetarenko et al. 2015 using Very Large Array (VLA) at different frequencies. The possible correlation between X-ray characteristics and radio flares are explored in section 3.4.

3 RESULTS

We have performed a detailed spectral and temporal analysis of the source V404 Cyg, and the results of the same are presented here.

3.1 Spectral evolution

We carry out the spectral analysis, by fitting the energy spectrum in 0.5 - 150 keV, using several models. The spectral fit with all the spectral components for one of the simultaneous observations (i.e. day 10.01; MJD 57198.01), has been shown in Figure 1. We find that the spectral fit using *diskbb*, *gauss* and *compTT* (see top panel of Figure 1) results in χ^2/dof of 791/689, and gives large residuals above 15 keV indicating the presence of a reflection component. We also could not constrain the *compTT* parameters. Hence, we replace *compTT* with the *pexrav* model which takes into account the reflection component and any high energy cut-off observed. This improves the fit and results in χ^2/dof of 699/687. The *diskbb* model is used for those observations where we find presence of a disc component in the low energy spectrum. We also find evidence of prominent Fe line emission since day 3 (i.e. MJD 57191) during seven out of the entire twenty observations, and it is modeled using *gauss*. The inclination angle of the disc has been estimated as 56±4° by Shahbaz et al. 1994, and we refer to the same. The final model used is *wabs*(diskbb+gauss+pexrav)* as shown in the bottom panel of Figure 1.

Figure 2 represents the variation of the X-ray flux in 0.5 - 10 keV and 15 - 150 keV (panels a and b respectively), the radio flux (panel c) observed by RATAN-600 (Trushkin et al. 2015b), variation of hardness ratio (panels d and e) and fractional rms variability estimated from XRT observations in the frequency range of 0.1 - 20 Hz (panel f). The data points corresponding to the XRT observations are shown in red cross type points, whereas BAT in magenta box type points and the simultaneous XRT-BAT observations are indicated in blue open circular points. Error bars for all the observed/estimated parameters are also included. Some of the observations have error bars smaller than the symbol size. The different radio flares reported have been marked as F1, F2, F3. Around sixteen flares in X-rays have been detected by INTEGRAL (see Rodriguez et al. 2015 and INTEGRAL public data products), with flux > 6 Crab (i.e. > 990 counts/sec in 20 - 40 keV). Amongst these flares, we

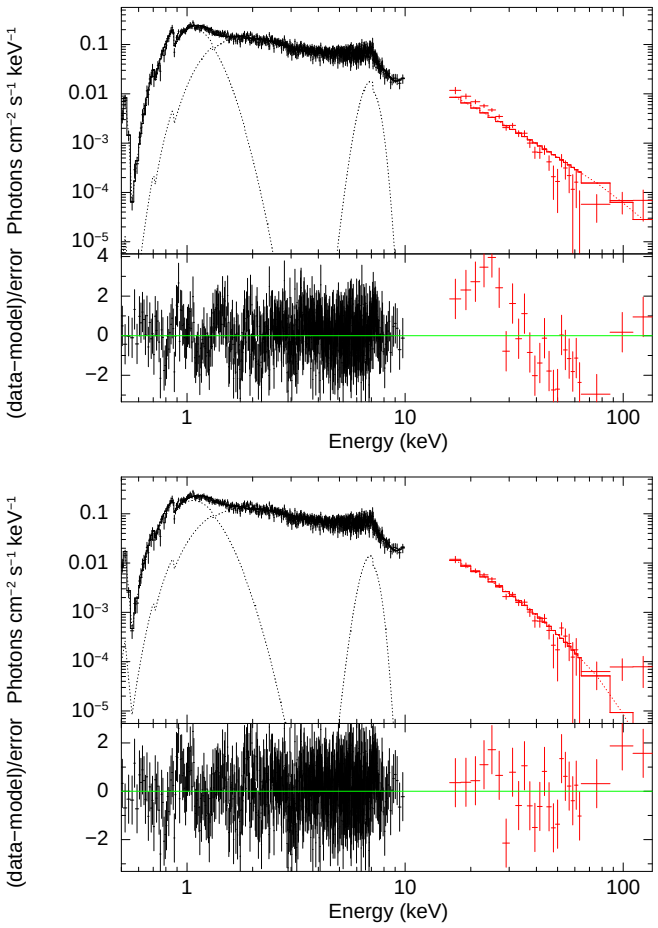

Figure 1. Spectral fit for simultaneous XRT and BAT observation on day 10.01 (MJD 57198.01) over the energy range of 0.5 - 150 keV, using the model *wabs*(diskbb+gauss+compTT)* in top panel and *wabs*(diskbb+gauss+pexrav)* in bottom panel. These fits indicate the presence of disc and Fe line components. The solid lines represent the fit to the data, while the dotted lines denote the model components. The BAT spectra has been re-binned by 10 counts/bin above 60 keV for better representation.

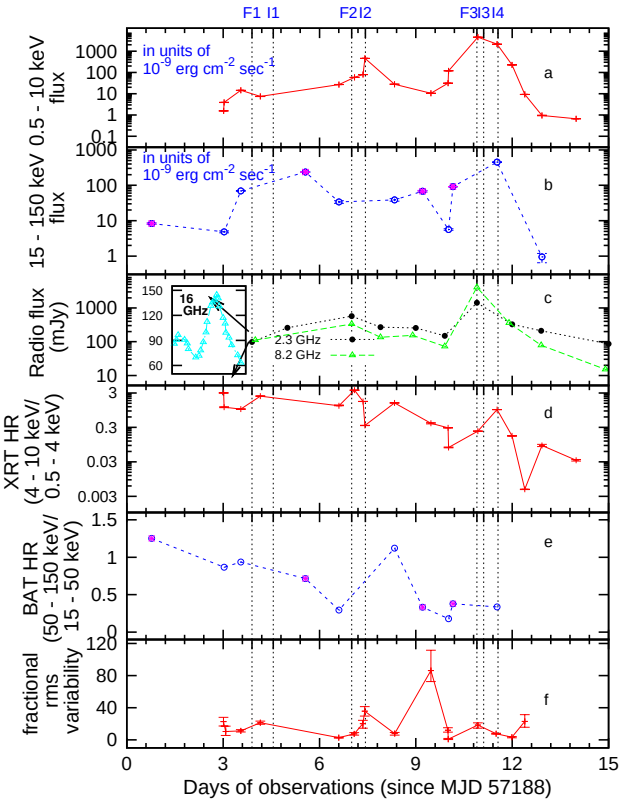

Figure 2. Variations of integrated XRT flux (a), BAT flux (b), Radio flux (c), Hardness ratios for XRT (d), Hardness ratios for BAT (e) and fractional rms variability in % (f) for XRT, are shown in different panels of this plot. Here XRT observations are shown in red cross, BAT observations by magenta box and simultaneous XRT+BAT observations by blue open circular points whereas radio flux are shown by black dots and green diamond points. Error bars for the different data points are also marked, and some of the observations have error bars smaller than the symbol size. The Radio flare detected by AMI-LA at 16 GHz during day 4 (i.e. MJD 57192) has been shown in the inset of the panel c, where the observations (cyan diamond points) are quoted in hours scale. F1, F2 and F3 represent the radio flares observed and I1, I2, I3 and I4 denote the X-ray flares detected by INTEGRAL. In the X-axis of the figure, day 0 corresponds to MJD 57188.

have represented in Figure 2, those flares which are closer to the X-ray flares we obtained from SWIFT analysis, and they have been indicated as I1, I2, I3 and I4. Variations of the different spectral parameters are shown in Figure 3, with representation of data points similar to Figure 2. In Table 1 we present model fitted spectral parameters from all the observations.

In the beginning of the outburst for a few observations (i.e. days 0.77, 3.01 and 3.03), we find that the spectra can be fitted well by a powerlaw. For uniformity, we have modeled the spectra with *pexrav*, which indicates lack of cut-off and reflection components for these observations. The observations after 3 days of the outburst (i.e. since MJD 57191.54), require a *diskbb* model along-with the *pexrav* model to fit the data, implying the presence of a soft disc and reflection component together-with the signature of high energy cut-off for simultaneous XRT and BAT observations.

We observe a similar spectral nature with the presence of both disc and hard components for all the observations considered, except for a few. During days 4.16, 6.40, 7.08 and 10.93, the XRT spectrum fits well with the *pexrav* without any *diskbb* component. We notice that this intermittent absence of disc component takes place just after a radio flare (see section 4) and makes this source very different from most of the other black hole transients.

We find that since day 3.54 (see also Table 1), the spectral fits for all the observations (except days 12 and 13) in the low energy range of 0.5 - 10 keV, require a model corresponding to absorption along-with the *diskbb* or/and *pexrav*, and *wabs* models. This absorption feature has been taken care using the *pcfabs* model, with the covering fraction varying between 0.5 and 0.95, to fit the spectral data. As an example for day 10.00, we find that the inclusion of *pcfabs* improves χ^2/dof from 918/667 to 725/665 for the low energy XRT spectral fit, suggesting this absorption characteristic to be statistically significant. In addition to this spectral absorption, we observe absorption lines of peak energy $\sim$ 0.67 keV with width 0.1 keV on days 6.60 and 8.34, while $\sim$ 9 keV absorption line of width $\sim$ 0.78 keV is observed on the 10th

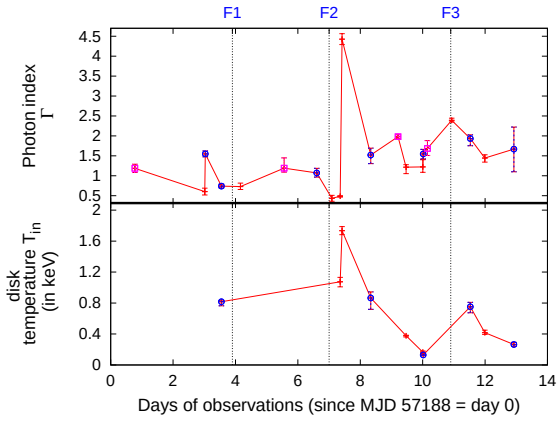

Figure 3. Evolution of the spectral parameters along-with their error bars, during the outburst for XRT (red cross points) and BAT (magenta box type points) observations. Simultaneous observations have been marked in blue open circular points. In the X-axis of the figure, day 0 corresponds to MJD 57188.

day of observations. We model both of these lines[6] using *gabs*.

Although we did observe the contribution from Keplerian disc for a few observations, Figure 3 and Table 1 indicate that the variation of disc parameters is random. The disc temperature is observed to vary between 0.16±0.01 keV to 1.73±0.05 keV. We note that the disc temperature is around 0.1 keV to 0.3 keV for few observations (although XRT spectra are modelled from 0.5 keV onwards), but these observations also have large contribution of the soft flux. The spectral fits show a significant presence of a disc component during these observations, say with the χ^2/dof improving from 1039/667 to 725/665 on day 10.00. The lower value of temperature could be an estimate of the physical disc temperature due to the extrapolation of the fit to the spectra. Also, the variation in the uncertainty of disc temperature is lesser than the disc temperature itself.

We find that the photon index has a random variation between 0.43±0.07 to $4.43^{0.27}_{-0.14}$ (Figure 3 and Table 1), unlike the typical black hole sources where it exhibits continuous increase (e.g. GX 339−4 (Belloni et al. 2005), GRO J1655−40, XTE J1550−564, XTE J1650−500 (Shaposhnikov & Titarchuk 2009), XTE J1859+226 (Radhika & Nandi 2014), IGR J17091−3624 (Iyer et al. 2015)) during the initial phase of the outburst.

The XRT flux (0.5 - 10 keV) reaches to a maximum on day 10.93 (Figure 2), with an observed value of 4560.0±23.3 $\times10^{-9}$ erg cm^{-2} sec^{-1} corresponding to a luminosity of 2.96±0.4 $\times10^{39}$ erg sec^{-1} for the source distance of 2.39 kpc (see also section 1) estimated by Miller-Jones et al. 2009. On day 11.5, the 0.5 - 10 keV X-ray flux is 2130.7±6.5 $\times10^{-9}$ erg cm^{-2} sec^{-1} and the 15 - 150 keV BAT flux achieves a peak (Figure 2) of 453.1±5.1 $\times10^{-9}$ erg cm^{-2} sec^{-1} (see also Segreto et al. 2015). The corresponding peak BAT luminosity is 0.29±0.04 $\times10^{39}$ erg sec^{-1}. The total X-ray flux in 0.5 - 150 keV during day 11.5, is found to be 2583.8±8.24 $\times10^{-9}$ erg cm^{-2} sec^{-1}, which is equivalent to a luminosity of 1.68±0.08 $\times10^{39}$ erg sec^{-1}. Segreto et al. 2015 reported a maximum luminosity of the order of 10^{39} erg sec^{-1} for a 12M$_\odot$ central source (see section 4).

[6] We observe an indication for these absorption lines, but due to lower photon statistics (because of less effective area of XRT) an accurate modeling of the same is not possible.

3.2 Temporal evolution

During the initial days, the XRT power density spectrum shows only broad-band noise and has higher fractional rms variability. For days 3.54 and 7.08, we find that the PDS has a powerlaw noise, and the fractional rms variability is around 7±2 % to 11^{1}_{-2}%. The rest of the PDS has a broad-band noise. The XRT rms achieves a minimum of $0.79^{0.5}_{-0.3}$% on day 10.01 (see panel f of Figure 2). A powerlaw shape of the XRT-PDS is observed during day 11 also, but with the rms decreased to $\approx7.6^{0.4}_{-0.5}$%.

The INTEGRAL observations performed on days 0 and 2 have reported presence of significant low frequency QPOs in their PDS (Prosvetov & Grebenev 2015) at 0.124 Hz and 0.251 Hz. Low frequency QPOs have also been observed by FERMI-GBM (Jenke et al. 2015, 2016) during days 4 and 5. We did not find any signature of significant (>3σ) QPOs in the PDS of both XRT and BAT, for the observations considered. Although, Motta et al. 2015a reported about the detection of a 3.1σ significant QPO of 1.7 Hz on day 3.03, we do not find any clear detection of this QPO during this observation but weak features around 0.12 Hz and 0.25 Hz are evident (see the 1st panel of Figure 4). We find that during this period and also when INTEGRAL/FERMI detected QPOs, the PDS generated for the minimum time resolution of the SWIFT-BAT observations also do not show significant detection of QPOs but only a broad-band noise. FERMI has detected mHz QPOs during days 4 and 5 (Jenke et al. 2016). The power spectrum generated for day 4.15, shows a weak feature/peaked component at 0.09 Hz (2nd panel of Figure 4). The following XRT observation on day 6.60 does not indicate any signatures of peaked components or QPOs but has only broad-band noise (3rd panel in Figure 4).

3.3 Hardness-intensity and rms-intensity diagrams

The hardness intensity diagram (HID) and rms-intensity diagram (RID) are generated for XRT observations as shown in top panel of Figure 5. Since Fe line emission is observed only for seven observations, we have estimated the flux in each energy band by excluding the contribution from the Fe line, so as to have uniform estimation throughout. We find that during the initial days both the XRT and BAT hardness ratios remain high (see, panels d and e in Figure 2) at a lower flux level (top panel of Figure 5). Spectral modelling implies the spectra to be dominated by hard emission without any presence of a disc emission, and the temporal properties imply that the fractional rms variability is higher (> 20%) during this period (Figure 2 and bottom panel of Figure 5). The low frequency QPOs observed by INTEGRAL during the same period, are similar to the type C QPOs observed in most of the black hole sources (Casella et al. 2004). These spectral and temporal characteristics with variations, suggest the source to be in the hard state during the initial days.

Table 1. Best fitted model parameters representing the different spectral properties. Here 'Day' corresponds to days since MJD 57188 (day 0), T_{in} is disc temperature, Γ is photon index, fE is fold energy in keV and rel_{refl} is the reflection factor and EW is equivalent width of the Fe line. Both the disc flux and hard flux, are quoted in units of 10^{-9} erg cm^{-2} sec^{-1}. The spectral parameters mentioned are same as that represented in Figure 3. The contribution of disc flux is estimated in 0.5 - 10 keV energy range (i.e. range A), while that of the powerlaw flux is estimated in 0.5 - 10 keV (range A) for the observations with only XRT data, and in 15 - 150 keV (range B) for the rest. The parameters of fE and rel_{refl} are quoted only for the simultaneous observations where the cut-off and reflection features are statistically significant.

Day	T_{in}	disc flux	Γ	powerlaw* flux		line energy	EW	fE	rel_{refl}	χ^2/dof
	(keV)	(range A)		(range A)	(range B)	(keV)	(keV)	(keV)		
0.77	-	-	1.18 ± 0.1	-	8.78 ± 0.41	-	-	-	-	47.43/3
3.01	-	-	$0.60^{0.08}_{-0.09}$	1.43 ± 0.03	-	6.60 ± 0.08	$0.77^{+0.22}_{-0.19}$	-	-	253/28
†3.03	-	-	$1.55^{0.08}_{-0.09}$	-	$4.83^{0.04}_{-0.05}$	-	-	-	-	286/41
†3.54⋆	$0.82^{0.01}_{-0.05}$	5.15 ± 0.04	$0.74^{0.09}_{-0.04}$	-	69.44 ± 1.0	-	-	$42.43^{+0.05}_{-0.03}$	-	887/111
4.16⋆	-	-	$0.73^{0.09}_{-0.07}$	7.49 ± 0.07	-	$6.26^{0.1}_{-0.06}$	$1.15^{+0.22}_{-0.19}$	-	-	933/75
5.56⋆	-	-	$1.19^{0.2}_{-0.1}$	-	241.28 ± 2.7	-	-	-	-	43/71
†6.60⋆	-	-	1.07 ± 0.08	-	33.81 ± 3.1	6.84 ± 0.08	0.30 ± 0.07	$18.81^{+4.2}_{-3.3}$	0.67 ± 0.23	912/109
7.08⋆	-	-	0.43 ± 0.07	55.13 ± 0.38	-	6.73 ± 0.04	$0.47^{+).07}_{-0.06}$	-	-	931/82
7.35⋆	$1.07^{0.6}_{-0.7}$	16.68 ± 0.01	$0.48^{0.03}_{-0.02}$	62.81 ± 0.27	-	-	-	-	-	1405/91
7.41⋆	1.73 ± 0.05	304.92 ± 1.51	$4.43^{0.27}_{-0.14}$	155.19 ± 3.1	-	-	-	-	-	973/71
†8.34⋆	$0.86^{0.15}_{-0.08}$	4.95 ± 0.05	$1.52^{0.18}_{-0.21}$	-	36.53 ± 3.0	6.59 ± 0.05	$0.71^{+0.10}_{-0.07}$	$100.90^{+14.8}_{-12.7}$	10.01 ± 0.87	832/95
9.21⋆	-	-	1.98 ± 0.05	-	68.15 ± 3.7	-	-	-	-	32/36
9.47⋆	0.38 ± 0.01	5.22 ± 0.19	$1.22^{0.22}_{-0.16}$	5.35 ± 0.13	-	6.43 ± 0.04	$0.23^{+0.4}_{-0.05}$	-	-	311/34
10.00⋆	$0.16\pm0.01^{!}$	18.54 ± 0.49	$1.22^{0.3}_{-0.1}$	12.73 ± 0.12	-	-	-	-	-	725/66
†10.01⋆	$0.13\pm0.01^{!}$	105.91 ± 3.3	$1.54^{0.2}_{-0.1}$	-	5.64 ± 0.28	$6.9^{\$}$	0.29	$16.95^{+5.01}_{-2.32}$	$0.97^{0.15}_{-0.16}$	699/68
10.15⋆	-	-	$1.68^{0.19}_{-0.17}$	-	94.05 ± 1.2	-	-	-	-	20/37
10.93⋆	-	-	2.39 ± 0.05	4560.0 ± 23.2	-	-	-	-	-	1201/75
†11.5⋆	$0.75^{0.05}_{-0.07}$	300.47 ± 3.57	$1.93^{0.27}_{-0.18}$	$2130.6^{6.44}_{-6.47}$	$453.11^{5.2}_{-5.0}$	-	-	$60.79^{+11.9}_{-16.8}$	1.39 ± 0.04	899/127
11.9⋆	$0.42^{0.03}_{-0.02}$	160.11 ± 1.1	1.44 ± 0.1	66.28 ± 0.76	-	-	-	-	-	664/61
12.39	0.49 ± 0.06	0.366 ± 0.09	4.52 ± 0.12	$8.97^{0.15}_{-0.59}$	-	-	-	-	-	397.56/3
†12.92	$0.26^{0.03}_{-0.02}{}^{!}$	0.78 ± 0.03	$1.66^{1.0}_{-0.6}$	-	$0.91^{0.09}_{-0.03}$	-	-	-	-	306/33
13.99	0.25 ± 0.03	0.37 ± 0.05	3.04 ± 0.4	0.29 ± 0.02	-	-	-	-	-	185.71/1

* - The *pexrav* model is used for the spectral fit to obtain the contribution from the powerlaw/hard flux.
† - observations with simultaneous XRT and BAT data.
$ - line energy is kept fixed, so as to constrain the parameters.
⋆ - The *pcfabs* model is included while modeling the spectra.
• - observations with residuals at Si and Au edges of XRT show $\chi^2/dof > 1.2$
! - Significant presence of disc component, with increased contribution of soft flux

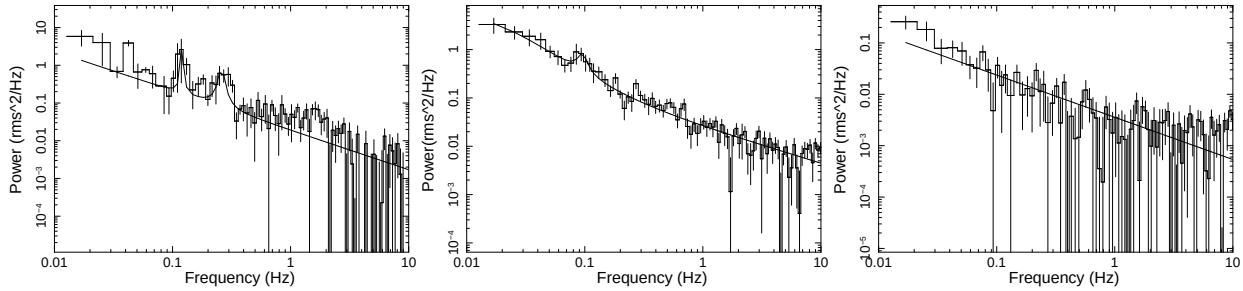

Figure 4. Power density spectra for the observations on days 3.03, 4.15 and 6.60 respectively. These PDS show that there is no clear detection of QPOs but have only weak peaked components. The solid line shows the complete fit to the PDS.

The XRT HID is later observed to show random fluctuations with occasional decrease in hardness ratio, resulting in a circular track during the intermediate states. For this period, multiple radio ejections (marked in grey circles in Figure 5) have occurred and the variations of the spectral parameters are random (Figures 2 and 3). The fractional rms variability is also observed to show a random variation (bottom panel of Figure 5) during this period of outburst. Although the spectral and temporal parameters suggest that this duration belong to an intermediate state, due to the random variation observed it is difficult to differentiate the states into hard intermediate and soft intermediate. This prohibits the HID to follow the typical 'q-shape' (Belloni et al. 2005; Dunn et al. 2010 and references therein) observed in other outbursting black hole sources like GX 339−4 (Belloni et al. 2005; Nandi et al. 2012). During the same period, the BAT hardness ratio is observed to decrease from 1.25 to 0.3 (panel e of Figure 2).

As the source flux begins to decline since day 11.99, the hardness ratio is observed to decrease (Figure 2 and top panel of Figure 5). The XRT HID implies that during this period the source transits to soft state, when the fractional rms variability is also observed to decrease (bottom panel of Figure 5). For the days 12 and 13, although the spectra have hardness ratio of <0.09, the PDS implies a flat-top noise with higher fractional rms of >47%, and the rms variability is observed to be larger up-to a frequency of 60 Hz. Hence we do not indicate these observations either in the RID or Figure 2. Thus the XRT HID and RID deviate from the typical behaviour, due to the random variation observed during the hard and intermediate states[7].

3.4 X-ray characteristics during multiple radio flares

We observe that during day 3.54, the 0.5 - 10 keV flux increases to 14.5±0.07 × 10^{-9} erg cm^{-2} sec^{-1} (Figure 2). The XRT hardness ratio and fractional rms variability are observed to decrease (Figure 2, 5) w.r.t the previous observations. Almost 12 hrs later on day 4 (i.e. MJD 57192), a radio flare of flux 140 mJy (see inset figure in panel c of Figure 2)

[7] No random variation has been observed for most of the outbursting sources during the initial phase of the outburst, except in SIMS (e.g. GX 339−4 (Belloni et al. 2005; Nandi et al. 2012), XTE J1859+226 (Homan & Belloni 2005; Radhika & Nandi 2014)).

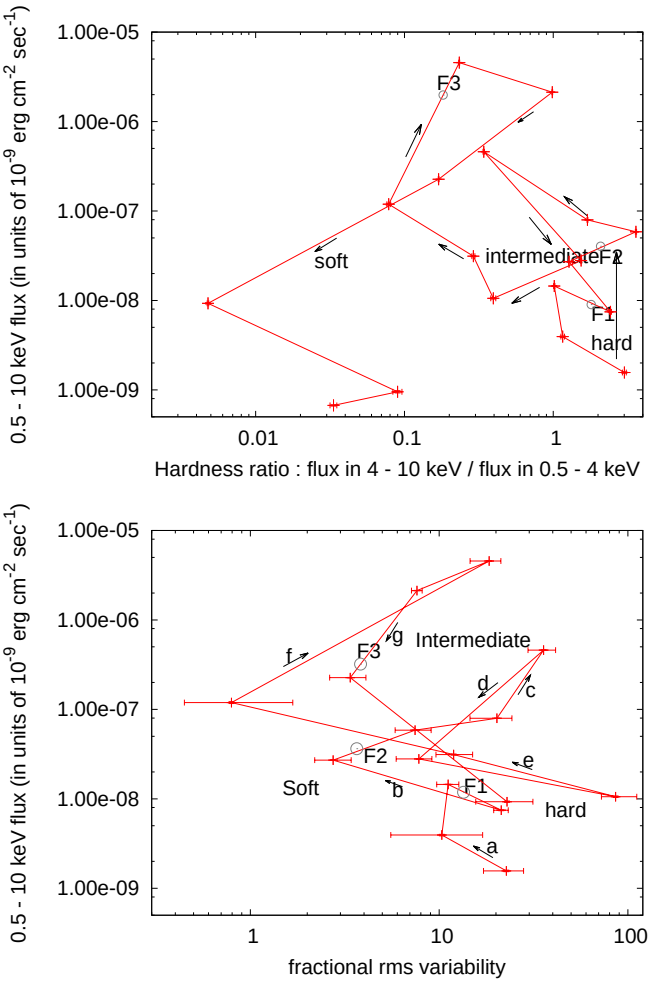

Figure 5. A plot of the hardness intensity diagram (top panel) and rms-intensity diagram (bottom panel) based on XRT data. The hardness ratio has been estimated as ratio of flux in 4 - 10 keV to 0.5 - 4 keV. The flux values in different bands have been estimated by excluding the contribution of the Fe line emission. The radio flares (F1, F2 and F3) are also indicated as grey circles closer to the next X-ray observation. The arrows marked from a to g in the bottom panel indicate the direction of the evolution of the RID. The fractional rms variability has been estimated in the frequency range of 0.1 - 20 Hz.

has been observed at 16 GHz using AMI-LA (Mooley et al. 2015a,b). We denote this flare as F1 in Figure 2, which is rapid and has an oscillating appearance. RATAN-600 also reports the detection of a radio flux of 112.25 mJy at 8.2 GHz during the same period (Trushkin et al. 2015b). The INTEGRAL observation on day 4.5 has reported an X-ray flaring activity (marked I1 in Figure 2) closer to this period (Ferrigno et al. 2015). But there is no SWIFT observation available on this day.

We find that the 15 - 150 keV flux, the BAT hardness ratio and XRT fractional rms decreases (Figure 2) during day 6.60 with respect to the previous observations. It can be also noted from panel c of Figure 2 that the radio observations indicate an increase in flux to 336.24 mJy (flare F2) at 8.2 GHz on day 7 (Tetarenko et al. 2015; Trushkin et al. 2015b). After the radio flare, we find that the 0.5 - 10 keV flux increases to $460.11\pm3.16 \times 10^{-9}$ erg cm^{-2} sec^{-1} (panel a of Figure 2) on day 7.41, during which both disc temperature and photon index are found to have increased (Figure 3). This increase in XRT X-ray flux is in positive correlation with the X-ray flare (I2 in Figure 2) observed by INTEGRAL.

Similar characteristics are observed during the peak radio flare (F3 in Figure 2) on day 11. In Figure 6 we represent the variations of the 15 - 150 keV BAT spectra before and after the radio flare. We find that during the observation on day 10.01 (spectra indicated in green colour and open circular points in Figure 6), the 15 - 150 keV BAT flux, the BAT hardness ratio and the XRT fractional rms variability (panels e and f of Figure 2) decreases during this observation. Thus a significant decrease in the hard flux is observed with respect to the previous observation on days 9.21 (red star points in Figure 6) and 8.34 (spectra in black colour with point type of cross). The radio observations indicate an increase in the flux to 4085.1 mJy at 8.2 GHz on day 11, giving rise to a peak flare (F3 in Figure 2) with inverted spectrum at low frequencies (Trushkin et al. 2015a). Following this event, both XRT and BAT fluxes are observed to increase (spectra in blue colour with box type points) and attain a maximum during days 10.93 and 11.5 respectively (see Figure 2). INTEGRAL observations also report peak X-ray flares (I3 and I4) during this period. The possible connection between the X-ray characteristics and radio flares during all these observations are discussed in section 4.

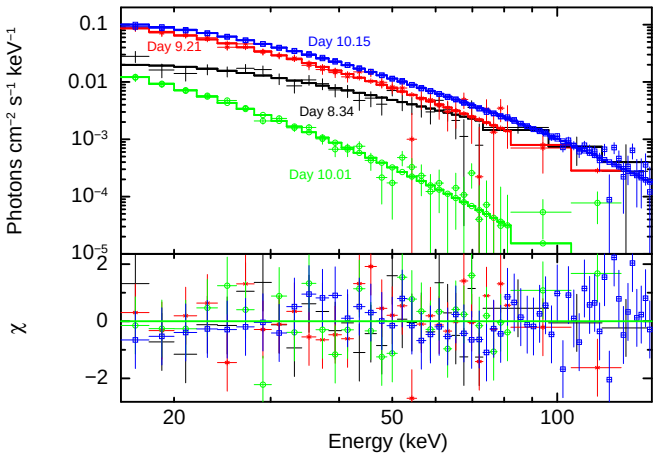

Figure 6. Evolution of the 15 - 150 keV spectra during the period of days 8.34 to 10.15, indicating decrease in flux almost 24 hrs before the peak radio flare observed on day 11. The BAT spectra for days 8.34, 9.21 and 10.01 have been re-binned above 60 keV for better representation.

3.5 Evolution of the Fe line emission

The spectral analysis suggest the presence of an Fe line component during seven observations. In order to understand the relativistic effects on this line, we modeled the line profile with *diskline* (Fabian et al. 1989) model. The fit results show the parameter of the equivalent width to be of the order of 10^{-7} keV, which is not appropriate. This also could be giving an indication that the Fe line is not originating from the disc and has a different source of origin (see section 4). In order to consider the broadening of the Fe line, we decide to model it with the *gauss* only.

We observe that the peak energy of the Fe line is varying from 6.26 keV to 6.9 keV, and the line energy evolves as shown in Figure 7. During the first XRT observation on day 3.01, when the source exists in the hard state without any signature of the disc component, we observe the Fe line to have an equivalent width of 0.77 keV (spectra shown in black colour and dot points in Figure 7). We find that this line contributes a fraction of 0.08 of the total flux. The spectral fit for this observation does not show any absorption features.

During days 4.16 to 10.01, the equivalent width of the Fe line is observed to be varying between 0.23 keV and 1.15 keV. The fractional contribution of the Fe line flux to the total flux, is found to be varying from a minimum of 0.01 to a maximum of 0.12. We find that during these observations, the spectral fits also show absorption features, which has been taken into account using the *pcfabs* model. This period belongs to the intermediate state of the source. The Fe line observed on day 9.47 is found to be very narrow and has an equivalent width of 0.23 keV (magenta spectra with box type points in Figure 7). We observe from Figure 7 that the flux of the Fe line observed on days 3.01 and 9.47 are lesser than that for the other observations, with a maximum of $3.38\pm0.2 \times 10^{-9}$ erg cm^{-2} sec^{-1} on day 7.08 (see spectra with blue open circles in Figure 7). We discuss the possible reasons for the evolution of the Fe line in section 4.

Multiple Fe lines of different energies have been also detected for this outburst of V404 Cyg by King et al. 2015 based on Chandra observations during days 7 and 8. They find presence of Fe K_α of 6.39 keV, K_β of 7.058 keV, Fe XXV of 6.63 and 6.682 keV, and Fe XXVI of 6.973 keV. Since XRT has a poor energy resolution and less effective area in comparison with Chandra-HETG, we are not able to resolve into the different narrow Fe lines. Yet, it might be possible to identify the Fe lines obtained from XRT observations, by comparing their centroid energy with the fluorescence lines observed using Chandra. The narrow line which we have observed from the XRT observation during day 9.47 at 6.43 keV might be Fe K_α, and that during day 10.01 at 6.9 keV might be Fe XXVI. The broad lines observed during the other days could be a possible blend of some of the other Fe line emissions.

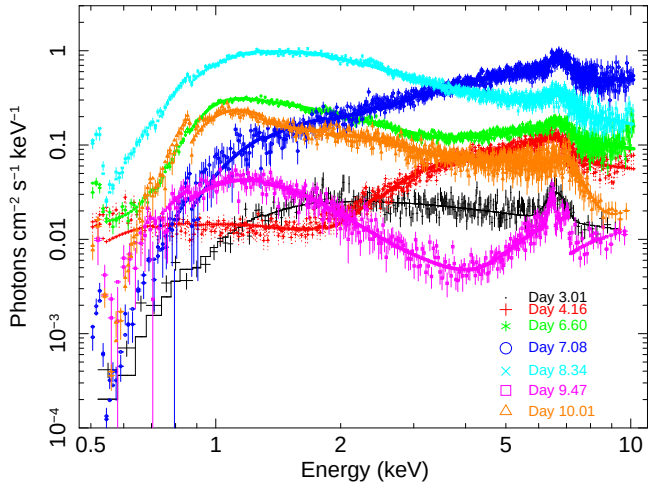

Figure 7. Evolution of the Fe line emission in the 0.5 - 10 keV XRT spectra. Although there are twenty observations, the signature of Fe line is observed only for seven of these.

4 DISCUSSIONS AND CONCLUSIONS

In this paper, we have studied the spectral and temporal variations of the source GS 2023+338 (V404 Cyg) based on the SWIFT XRT and BAT observations, during the initial days of the June 2015 outburst. It has been understood that outbursting black hole sources undergo spectral state transitions during their outburst phase. As the outburst progresses, based on the contributions of the thermal (Keplerian disc) and non-thermal emission (Compton corona), the source occupies different spectral states of 'hard, hard intermediate, soft intermediate and soft'. These states can be identified based on the variations of the spectral photon index, hardness ratio, the fractional rms variability and the types of QPOs (Casella et al. 2004; Belloni et al. 2005; Debnath et al. 2008; Munoz-Darias et al. 2011; Nandi et al. 2012). During the end of the outburst the source passes through the soft intermediate, hard intermediate and hard state, and thus forms a 'q-profile' in the hardness intensity diagram (Belloni et al. 2005; Dunn et al. 2010; Nandi et al. 2012; Corral-Santana et al. 2016 and references therein). In this paper, we classify the spectral states of the source V404 Cyg based on the observed variations of the spectral and temporal parameters (see section 3.3 and below) with reference to Belloni et al. 2005; Remillard & McClintock 2006; Debnath et al. 2008; Nandi et al. 2012.

These spectral and temporal characteristics, spectral states and evolution of the HID, can be understood based on several theoretical models like the two component advective flow model; (Chakrabarti & Titarchuk 1995). This model consists of a viscous Keplerian flow at the equatorial plane, and a less viscous sub-Keplerian flow which sandwiches the Keplerian flow. During the accretion phase, the sub-Keplerian flow may undergo a shock transition and form a hot, puffed-up dynamical Compton corona which inverse-Comptonize the soft photons from the disc to produce hard X-ray photons in the form of a power-law distribution. As the outburst begins, the matter in the sub-Keplerian flow dominates giving rise to a hard state with a powerlaw spectrum in the higher energies. When the matter flows inward, the flow in the Keplerian disc increases giving rise to a multi-coloured disc blackbody emission resulting in the contribution of soft photons to increase. This will give rise to the hard intermediate state. As the source reaches the soft intermediate state, the contribution of the Keplerian disc emission increases since the sub-Keplerian flow decreases. Later while in the soft state the Keplerian emission dominates and the sub-Keplerian has minimal contribution to the total flux. Recently, attempts have been made for several black hole binaries to classify the spectral states based on the instantaneous variation of accretion rates of the Keplerian and sub-Keplerian flow, shock parameters etc. (see Mondal et al. 2014b; Debnath et al. 2015b,a; Jana et al. 2016 and references therein) within the context of this two component model. Similar studies for V404 Cyg using this model will be performed later and the results will be presented elsewhere.

Based on these general understandings of outbursting black hole binaries, we study the properties of the source V404 Cyg during its June 2015 outburst. Observations by INTEGRAL reported by Rodriguez et al. 2015 suggests the presence of a cut-off powerlaw describing the thermal Comptonization process and additional powerlaw at energies above 100 keV. They associate the flaring activity with the hard X-ray spectral changes and note that the source remains harder during the X-ray flares. In this paper, we find that the variations observed for V404 Cyg in the spectral parameters, X-ray flux, hardness ratio and the fractional rms variability suggest that the source has occupied different spectral states during the outburst.

We observe that during the initial days of the outburst, the spectral characteristics suggest a dominant hard emission (Figure 2), described by a powerlaw without any signature of cut-off and reflection components in the spectra. The hardness ratio is observed to remain high and the HID indicates a random variation during these observations. The temporal characteristics also imply that the fractional rms variability remains high during these days (Figures 2,5). Thus the spectral and temporal properties during this period suggest the source to have occupied a hard state.

The INTEGRAL satellite which has larger effective area and better time resolution has observed significant QPOs on days 0 and 2 (Prosvetov & Grebenev 2015) during which there are no SWIFT-XRT observations. The PDS of BAT observation on day 0 also does not show presence of QPOs. Till date there has been no detailed description of the INTEGRAL observations of QPOs in a manuscript, except an Astronomer's Telegram (Prosvetov & Grebenev 2015) which we have referred in this manuscript. Contrary to Motta et al. 2015b, we do not observe a significant QPO at 1.7 Hz during day 3.03 (i.e. MJD 57191.03) of the SWIFT observations but a weak peaked component is noted at lower frequencies (see Figure 4 and section 3.2).

Observations after 3 days imply a significant contribution to the spectrum from the disc (see bottom panel of Figure 3, Table 1), along-with the hard emission which exhibits a cut-off and reflection component between 15 keV and 30 keV. This presence of a soft disc/spectral softening is not observed by INTEGRAL/FERMI probably due to their energy range coverage. We observe intermittent absence of both the disc and the Fe-line emission during the outburst. The hardness ratio is observed to decrease occasionally during this period (panels d and e of Figure 2). The hardness intensity diagram, shows random fluctuations (top panel of

Figure 5) and hence do not exactly follow the 'q-shape' observed for most of the black hole transients (Belloni et al. 2005; Dunn et al. 2010; Nandi et al. 2012; Radhika & Nandi 2014 and references therein).

The fractional rms variability is observed to exhibit a random variation as shown in bottom panel of Figure 5 which is dissimilar to that for most of the other sources like GX 339−4 (Munoz-Darias et al. 2011). Unlike the 1989 outburst where the power density spectra were observed to show a flat-top noise (Oosterbroek et al. 1997), for the 2015 outburst we find that the PDS have either broad-band noise or flat-top noise for most of the observations. The power spectrum is observed to exhibit powerlaw nature for a few observations (i.e. during days 3.54, 7.08 and 11.52), and also a decrease in fractional rms variability. All these characteristics suggest the period of days 3.54 to 11.9, to belong to an intermediate state. Weak mHz QPOs are detected based on FERMI-GBM observations during days 4 and 5 (Jenke et al. 2016) while in this state. We find that during the near simultaneous (w.r.t the FERMI observations) XRT observation on day 4.15, there is a weak peaked component present (see third panel of Figure 4).

The source is observed to attain its peak during this intermediate state. Based on BAT observations, it has been reported by Segreto et al. 2015 that the maximum luminosity of the source is of the order of 1.6×10^{39} erg sec^{-1} in 1 - 500 keV. We also obtain a value of 1.4×10^{39} erg sec^{-1} in the same energy band using *dummyrsp* in XSpec for the same BAT observation used by Segreto et al. 2015. Yet, when we incorporate the XRT spectrum, a significant contribution from the Keplerian disc (i.e. soft emission) is also observed to exist. Hence the total luminosity observed should be estimated by considering both the soft and hard emission spectrum, and it is found to be $1.68\pm0.08\ \times10^{39}$ erg sec^{-1} (see section 3 in 0.5 - 150 keV energy band. This value of the peak luminosity is observed to match with the Eddington luminosity expected for a source with mass > 10 $M_\odot$. Shahbaz et al. 1994 has reported the source mass to be of 12 $M_\odot$.

Observations since day 12 suggest that the hardness ratio decreases to its minimum (Figures 2 and 5), and the contribution from hard emission also declines (see Figure 2 and Table 1). Hence this period probably belongs to the soft state. We observe that during this outburst of the source, multiple radio flares have also been detected, as shown in Figures 2, 3 and 5. It is found that although on days 12 and 13 the spectra is softer, the PDS imply higher rms variability. This huge increase in rms power might be due to the dust scattering rings observed during this period (Beardmore et al. 2015).

We find that just before the detection of a radio flare, the spectral and temporal properties are changing. The energy spectra is observed to become softer indicated by either an increase in soft/XRT (0.5 - 10 keV) flux or decrease in hard/BAT (15 - 150 keV) flux, and the temporal properties imply a reduction in the fractional rms variability (Figures 2 and 5). This has been observed three times for this particular outburst of the source V404 Cyg. All the flares F1, F2 and F3 are preceded by such variations, and the X-ray flare is observed to attain a maximum following the event. Mooley et al. 2015a,b; Tetarenko et al. 2015; Trushkin et al. 2015b have suggested/reported these flares to be optically thin[8] at higher frequencies and observed them to be similar to the bright ejections from GRS 1915+105. Such changes in X-ray characteristics have been observed earlier for several Galactic black hole transients like XTE J1859+226, XTE J1550−564, H 1743−322 (see Fender et al. 2004, 2009; Miller-Jones et al. 2012; Radhika & Nandi 2014; Radhika et al. 2016 and references therein).

It has been understood for many black hole sources that the jet ejection/radio flare might be occurring due to the ejection of matter from the dynamical Compton corona (Chakrabarti 1999; Vadawale et al. 2001; Nandi et al. 2001 and references therein). This will result in the decrease of hard photons and fractional rms variability, and QPOs may not be observed in the power spectra. Detailed studies on this have been performed for GRS 1915+105 by Vadawale et al. 2001, and for other outbursting sources like XTE J1859+226, H 1743−322 etc. (Fender et al. 2004, 2009; Miller-Jones et al. 2012; Radhika & Nandi 2014; Radhika et al. 2016; Nandi et al. 2016).

The disc-jet coupling phenomenon has been understood based on theoretical studies by Blandford & Znajek 1977 and using simulations by McKinney & Gammie 2004; De Villiers et al. 2005 considering the black hole spin as the origin for jets, or based on poloidal magnetic field by Varniere & Tagger 2002. Further understanding of the jet ejection as mass loss from a hydrodynamical accretion disc due to the presence of centrifugal barrier (Chakrabarti 1999), and the collimation of jet (Spruit 1996; Fukue et al. 2001; Chattopadhyay et al. 2004; Chattopadhyay 2005) have also been studied in detail. Fender et al. 2004 have developed an unified model of the disc-jet coupling based on the observational results. The model states that a compact non-relativistic jet exists while in the hard and hard intermediate states, and during the transition from hard intermediate to soft intermediate state, a relativistic jet ejection occurs (see section 1 also).

Multiple radio flaring/jets have been observed during the transition to, and while in the soft intermediate states in other black hole transients like XTE J1859+226 (Fender et al. 2009; Radhika & Nandi 2014), XTE J1752−223 (Brocksopp et al. 2013). But for V404 Cyg, we observe multiple radio flaring just after the transition from the hard state to the intermediate state. The first radio flare (F1) which appears to be oscillating/variable, probably occurs during the transition from the hard state. Before this radio flare both the soft (XRT) and hard (BAT) flux increases (panels a and b of Figure 2), and this is because the dynamical Compton corona is relatively large in size and hot, so that even in the presence of outflow/jet (which is not very strong in this case), the disc is capable of producing hard energy and complete evacuation of the dynamical corona is not possible. Several works have been performed based on simulations, in order to understand the characteristics of variable/oscillating outflows/flares similar to the flare F1 of V404 Cyg (see Molteni et al. 1996, 2001; Das et al. 2014 and references therein).

The second and third flares (F2 and F3 respectively) are much stronger than the first flare (F1) and happen while in the intermediate states. In this case the disc is much

[8] http://www.sao.ru/Doc_en/SciNews/2016/Trushkin

closer (smaller corona) to the central engine, and matter will be evacuated from the dynamical corona in the form of jet/outflow. Hence both the soft and hard X-ray contribution decreases and the HID indicates X-ray radiation becomes relatively softer (see top panel of Figure 5, and Figure 6). Also we see X-ray flaring activity after the radio flare which can be understood in a two-component accretion flow paradigm (Chakrabarti & Titarchuk 1995, discussed earlier). Here, the sub-Keplerian flow has a much larger radial velocity than the Keplerian flow. Hence, after the radio flaring in intermediate state, quickly the evacuated dynamical corona is going to be filled by hot sub-Keplerian flow and this increases the hard X-ray activity. But after the first radio flare, we do not see any X-ray flare because the disc is more steady with higher rate of sub-Keplerian matter.

The random variation occurring in the HID could be probably due to some change of the accretion dynamics resulting in the ejection of multiple radio flares. It might be also happening that the hybrid flow comprising of Keplerian and sub-Keplerian (Chakrabarti & Titarchuk 1995) are being changed drastically due to the sudden change at the outer edge of the disc driven by some peculiar behaviour of the binary companion (see also Chakrabarti 2015 and references therein, for possible effects of the companion). To have a better understanding of the spectral and temporal behaviour of this source, one needs to do a more realistic modeling, which is beyond the scope of this paper, and calculate the flow parameters (say accretion rates, size of the central region, temperature of corona etc.; for an example see Debnath et al. 2015a; Iyer et al. 2015; Molla et al. 2016 and references therein for a few other sources). This may explain the random behaviour of HID in hard and intermediate states for this source. In fact, we do see some randomness in HID for outbursting X-ray binaries in intermediate states, because both Keplerian and sub-Keplerian accretion rates are comparable (see Mandal & Chakrabarti 2010; Debnath et al. 2015a; Molla et al. 2016 and references therein) or in other sense supply of hot electrons and soft photons are comparable which introduces non-linearity into the system. Our recent study (Radhika et al. 2016) of sources like GX 339−4, XTE J1859+226, H 1743−322 suggests the random variation during the transition from hard intermediate to soft intermediate state to be a 'local' phenomenon which results in ejection of radio flares. In V404 Cyg, we understand that the random variations are occurring for the hard and intermediate states also, and probably the change in accretion dynamics is taking place globally w.r.t the disc system, along-with 'local' changes which causes the ejection of matter in the form of radio flares.

It is observed that a few moments after the huge radio ejection (F3), the X-ray spectra becomes harder and the disc component is not observed. The spectral hardening might be occurring due to re-filling of matter in the dynamical corona. It is also possible that during the jet ejection, a portion of the inner part of the Keplerian disc has been ejected out resulting in non-detection of the disc component in the subsequent observation. We observe the disc emission again after a few hours during the next observation, since the Keplerian disc takes viscous timescale to refill and hence the re-emergence of soft/thermal emission. So more co-ordinated and dedicated multi-wavelength observations during massive radio flares in black hole sources can help to have a better understanding of similar observational features.

We find that during the observations when an Fe line is present while in the intermediate state, there are signatures of absorption for the low energy XRT spectra indicated by a partial covering absorption. This suggests the presence of an outflow/wind along-with the disc and corona. The Fe line observed based on our SWIFT analysis is found to have its peak energy varying from 6.26 keV to 6.9 keV. Presence of multiple Fe line emissions during the intermediate state of this source has been observed by Chandra-HETG (King et al. 2015) due to its very high spectral resolution in comparison to the SWIFT XRT. This variation of the Fe line energy suggests that the wind emission is strong enough to ionize the matter, and result in the emission of Fe lines at different energies.

Although the Fe-line obtained from our XRT analysis do not have a constant energy during the outburst but are varying randomly, we find that these lines differ from each other in their equivalent width and the flux. Those Fe lines which are observed after a radio flare, have more flux than the other lines. For example, the Fe line observed on day 4.16 has 10 times more flux than on day 3.01, and the observation of day 4.16 occurs after the first radio flare F1. Similarly the flux of Fe line on day 7.08 which takes place after the radio flare F2, is observed to be more than the previous observation. This suggests that stronger Fe line emission is associated with the wind emission, probably not related with the jet activity. We also note that the *diskline* model could not give a correct estimate of the line width, and this might have happened because the origin of the Fe line is not related to the disc.

During day 3.01 when the Fe line is observed in the hard state (where there is no detection of disc emission), probably the wind is optically thin and weak, that the spectra does not indicate strong signatures of absorption. Chakrabarti 1999; Mondal et al. 2014a suggest that the wind outflows can be originated from the centrifugal barrier of the two component model during the hard state of a source, and the rate of outflow is positively correlated with the accretion rate. Hence the Fe line observed during the hard state of V404 Cyg suggests its origin to be related to the wind outflow occurring from the centrifugal barrier. Possible mechanism for generation of winds due to heating of shock waves at the post shock region (centrifugal barrier) has been previously discussed in detail by Molteni et al. 1994 and references therein. Thus we understand that it is possible that wind/outflow is responsible for the Fe line emission observed during both the hard and intermediate states and, it may not be due to fluorescence similar to that observed for most of the outbursting black hole sources. Chakrabarti & Titarchuk 1995; Titarchuk et al. 2003 have discussed in detail about the possible connection between reflection profiles of Fe line and origin of wind outflows in stellar mass black hole binaries.

Most of the black hole binaries have an orbital period of a few hours, except a very few which have the orbital period in days (Remillard & McClintock 2006). The sources like XTE J1118+108, A 0620−00, XTE J1550−564 have orbital period in the range of 4 hrs to 37 hrs with their accretion rate varying from 10^{15} g sec^{-1} to 10^{16} g sec^{-1}. But sources which do not have an exact 'q-shape' in their HID have longer orbital periods. For an example, GRS 1915+105

has an orbital period of 33.5 days with peak accretion rate of 3.4×10^{18} g sec^{-1}. Although the source IGR J17091−3624 is similar to GRS 1915+105 in the variabilities it exhibits, the peak accretion rate is found to be lesser than that of the latter (Iyer et al. 2015). We understand that V404 Cyg which has an orbital period of 6.47 days (Casares et al. 1992), is probably not similar to most of the black hole sources (due to the deviation from 'q-shape' in HID and other characteristics discussed above) having a peak accretion rate of 3×10^{18} g sec^{-1} during its 2015 outburst. These findings show that, in low mass X-ray binaries, the sources which have shorter orbital period are having lower accretion rate than the sources which have longer orbital period and high accretion rate. But for the source Cygnus X-1 which belongs to a high mass X-ray binary with a longer orbital period of 5.9 days (Brocksopp et al. 1999), the peak accretion rate is only 6.7×10^{16} g sec^{-1}. This suggests that probably the accretion rate of a source depends not just on the orbital period but also on the characteristics of the binary system.

Based on the optical observations Kimura et al. 2016 have observed that during the 2015 outburst of the source V404 Cyg, due to its long orbital period, the accreted matter achieves the critical density for thermal disc instability at a smaller radius of the disc. The black hole sources with shorter orbital period of a few hours will have the thermal disc instability occurring at a larger outer radius of the disc. Rapid optical variations giving rise to oscillations are observed in the optical lightcurve of V404 Cyg by Kimura et al. 2016 which probably is due to the longer orbital period of the source. Although similar oscillations have been observed in the X-ray lightcurves of GRS 1915+105 and IGR J17091−3624, the reason/origin for the X-ray and optical oscillations might be different. It might be possible that the phenomenon responsible for the origin of the optical oscillations gets perturbed during the accretion process and is reflected in X-rays.

The random variation of the spectral parameters, hardness ratio, fractional rms variability, multiple radio flares, absorption features and the fact that the HID does not follow a 'q-profile' implies that the source V404 Cyg has a complex characteristic. These deviations categorize this source different from most of the outbursting black hole sources.

Thus, based on the spectral and temporal properties of the source GS 2023+338 (V404 Cyg) during its 2015 outburst, we arrive at the following conclusions.

- The spectral and temporal characteristics and the HID implies that the source occupies hard, intermediate and soft spectral states during this outburst.
- The HID deviates from the typical q-shape observed in most of the black hole transients. We find that the HID and the RID, have a random pattern while in the hard and intermediate states, and this also belongs to the period of multiple radio and X-ray flares. These observations imply that the source has a complex characteristic, unlike other black hole sources like GX 339−4, H 1743−322 etc..
- We observe weak peaked components in the power density spectra during the intermediate state of the source.
- We find that just before the detection of a radio flare/jet ejection, the energy spectra softens and the fractional rms variability decreases. This correlation between X-ray and Radio characteristics indicates the ejection of matter from the corona into jets.
- Absence of a disc is indicated just after the peak radio flare. This might be due to the possible evacuation of the inner part of the Keplerian disc.
- The spectral evolution indicates presence of absorption features for the low energy XRT spectral continuum, probably occurring due to outflow/wind emission. The evolution of the variable Fe line observed using SWIFT, during both the hard state (which has no signature of Keplerian disc emission) and the intermediate state, suggests that probably its origin is related to the wind, and not to the fluorescence emission from disc.

All these properties, imply that the source has a complex evolution during its 2015 outburst.

ACKNOWLEDGEMENTS

This research has made use of the data obtained through High Energy Astrophysics Science Archive Research Center on-line service, provided by NASA/GSFC. We are thankful to A. Beardmore for useful suggestions related to SWIFT-XRT data reduction. AN thanks GD, SAG, ISAC for continuous support to carry out this research. We thank the reviewer whose comments and suggestions have helped to improve the quality of this manuscript.

REFERENCES

Arnaud K. A., 1996, in Jacoby G. H., Barnes J., eds, Astronomical Society of the Pacific Conference Series Vol. 101, Astronomical Data Analysis Software and Systems V. p. 17
Barthelmy S. D., D'Ai A., D'Avanzo P., Krimm H. A., Lien A. Y., Marshall F. E., Maselli A., Siegel M. H., 2015, GRB Coordinates Network, 17929
Beardmore A. P., Altamirano D., Kuulkers E., Motta S. E., Osborne J. P., Page K. L., Sivakoff G. R., Vaughan S. A., 2015, The Astronomer's Telegram, 7736, 1
Belloni T., Homan J., Casella P., et al., 2005, A&A, 440, 207
Blandford R. D., Znajek R. L., 1977, MNRAS, 179, 433
Brocksopp C., Tarasov A. E., Lyuty V. M., Roche P., 1999, A&A, 343, 861
Brocksopp C., Fender R. P., McCollough M., et al., 2002, MNRAS, 331, 765
Brocksopp C., Corbel S., Tzioumis A., et al., 2013, MNRAS, 432, 931
Burrows D. N., et al., 2005, Space Sci. Rev., 120, 165
Casares J., Charles P. A., Naylor T., 1992, Nature, 355, 614
Casella P., Belloni T., Homan J., Stella L., 2004, A&A, 426, 587
Chakrabarti S. K., 1999, A&A, 351, 185
Chakrabarti S., 2015, Astronomy Reports, 59, 447
Chakrabarti S., Titarchuk L., 1995, ApJ, 455, 623
Chattopadhyay I., 2005, MNRAS, 356, 145
Chattopadhyay I., Das S., Chakrabarti S. K., 2004, MNRAS, 348, 846
Corbel S., Koerding E., Kaaret P., 2008, MNRAS, 389, 1697
Corral-Santana J. M., Casares J., Muñoz-Darias T., Bauer F. E., Martínez-Pais I. G., Russell D. M., 2016, A&A, 587, A61
Das S., Chattopadhyay I., Nandi A., Molteni D., 2014, MNRAS, 442, 251
De Villiers J. P., Hawley J. F., Krolik J. H., Hirose S., 2005, ApJ, 620, 878

Debnath D., Chakrabarti S. K., Nandi A., Mandal S., 2008, BASI, 36, 151
Debnath D., Mondal S., Chakrabarti S. K., 2015a, MNRAS, 447, 1984
Debnath D., Molla A. A., Chakrabarti S. K., Mondal S., 2015b, ApJ, 803, 59
Dunn R. J. H., Fender R. P., Körding E. G., Belloni T., Cabanac C., 2010, MNRAS, 403, 61
Fabian A. C., Rees M. J., Stella L., White N. E., 1989, MNRAS, 238, 729
Fender R. P., Belloni T., Gallo E., 2004, MNRAS, 355, 1105
Fender R. P., Homan J., Belloni T., 2009, MNRAS, 396, 1307
Ferrigno C., et al., 2015, The Astronomer's Telegram, 7662, 1
Fukue J., Tojyo M., Hirai Y., 2001, PASJ, 53, 555
Gazeas K., Vasilopoulos G., Petropoulou M., Sapountzis K., 2015, The Astronomer's Telegram, 7650, 1
Homan J., Belloni T., 2005, Ap&SS, 300, 107
Iyer N., Nandi A., Mandal S., 2015, ApJ, 807, 108
Jana A., Debnath D., Chakrabarti S. K., Mondal S., Molla A. A., 2016, ApJ, 819, 107
Jenke P., WIlson-Hodge C. A., Finger M. H., Paciesas W., Connaughton V., 2015, The Astronomer's Telegram, 7715
Jenke P. A., et al., 2016, preprint, (arXiv:1601.00911)
Kimura M., et al., 2016, Nature, 529, 54
King A. L., Miller J. M., Raymond J., Reynolds M. T., Morningstar W., 2015, ApJ, 813, L37
Kitamoto S., Tsunemi H., Miyamoto S., Yamashita K., Mizobuchi S., 1989, Nature, 342, 518
Krimm H. A., et al., 2013, ApJS, 209, 14
Kuulkers E., Wijnands R., Belloni T., Méndez M., van der Klis M., van Paradijs J., 1998, ApJ, 494, 753
Kuulkers E., Motta S., Kajava J., Homan J., Fender R., Jonker P., 2015, The Astronomer's Telegram, 7647, 1
Kylafis N. D., Belloni T. M., 2015, A&A, 574, A133
Magdziarz P., Zdziarski A. A., 1995, MNRAS, 273, 837
Makino F., 1989, IAU Circ., 4782, 1
Makishima K., Maejima Y., Mitsuda K., et al., 1986, ApJ, 308, 635
Mandal S., Chakrabarti S. K., 2010, ApJ, 710, L147
McKinney J. C., Gammie C. F., 2004, ApJ, 611, 977
Miller-Jones J. C. A., Jonker P. G., Dhawan V., Brisken W., Rupen M. P., Nelemans G., Gallo E., 2009, ApJ, 706, L230
Miller-Jones J. C. A., Sivakoff G. R., Altamirano D., et al., 2012, MNRAS, 421, 468
Mitsuda K., et al., 1984, PASJ, 36, 741
Molla A. A., Debnath D., Chakrabarti S. K., Mondal S., Jana A., 2016, MNRAS,
Molteni D., Lanzafame G., Chakrabarti S. K., 1994, ApJ, 425, 161
Molteni D., Ryu D., Chakrabarti S. K., 1996, ApJ, 470, 460
Molteni D., Acharya K., Kuznetsov O., Bisikalo D., Chakrabarti S. K., 2001, ApJ, 563, L57
Mondal S., Chakrabarti S. K., Debnath D., 2014a, Ap&SS, 353, 223
Mondal S., Debnath D., Chakrabarti S. K., 2014b, ApJ, 786, 4
Mooley K., Fender R., Anderson G., Staley T., Kuulkers E., Rumsey C., 2015a, The Astronomer's Telegram, 7658, 1
Mooley K., Clarke F., Fender R., 2015b, The Astronomer's Telegram, 7714, 1
Motta S., Homan J., Munoz-Darias T., et al., 2012, MNRAS, 427, 595
Motta S., Beardmore A., Oates S., Sanna N. P. M. K. A., Kuulkers E., Kajava J., Sanchez-Fernanedz C., 2015a, The Astronomer's Telegram, 7665, 1
Motta S. E., Beardmore A., Kuulkers E., Altamirano D., 2015b, The Astronomer's Telegram, 7694, 1
Munoz-Darias T., Motta S., Belloni T. M., 2011, MNRAS, 410, 679
Nandi A., Chakrabarti S. K., Vadawale S. V., Rao A. R., 2001, A&A, 380, 245
Nandi A., Debnath D., Mandal S., Chakrabarti S. K., 2012, A&A, 542, 56
Nandi A., et al., 2016, submitted
Natalucci L., Fiocchi M., Bazzano A., Ubertini P., Roques J.-P., Jourdain E., 2015, ApJ, 813, L21
Negoro H., et al., 2015, The Astronomer's Telegram, 7646, 1
Oosterbroek T., et al., 1997, A&A, 321, 776
Park S. Q., et al., 2004, ApJ, 610, 378
Prosvetov A. V., Grebenev S. A., 2015, The Astronomer's Telegram, 7726, 1
Radhika D., Nandi A., 2014, AdSpR, 54, 1678
Radhika D., Nandi A., Agrawal V. K., Seetha S., 2016, MNRAS, 460, 4403
Remillard R. A., McClintock J. E., 2006, ARA&A, 44, 49
Rodriguez J., et al., 2015, A&A, 581, L9
Roques J.-P., Jourdain E., Bazzano A., Fiocchi M., Natalucci L., Ubertini P., 2015, ApJ, 813, L22
Segreto A., Del Santo M., D'Aí A., La Parola V., Cusumano G., Mineo T., Malzac J., 2015, The Astronomer's Telegram, 7755, 1
Shahbaz T., Ringwald F. A., Bunn J. C., Naylor T., Charles P. A., Casares J., 1994, MNRAS, 271, L10
Shakura N. I., Sunyaev R. A., 1973, A&A, 24, 337
Shaposhnikov N., Titarchuk L., 2009, ApJ, 699, 453
Sivakoff G., Bahramian A., Altamirano D., Miller-Jones J., Russell D., 2015, The Astronomer's Telegram, 7763, 1
Spruit H. C., 1996, NATO ASI Series C., 477, 249
Tanaka Y., Lewin W. H. G., 1995, X-ray Binaries, pp 126–174
Tetarenko A., Sivakoff G. R., Young K., Wouterloot J. G. A., Miller-Jones J. C., 2015, The Astronomer's Telegram, 7708, 1
Titarchuk L., 1994, ApJ, 434, 570
Titarchuk L., Kazanas D., Becker P. A., 2003, ApJ, 598, 411
Trushkin S. A., Nizhelskij N. A., Tsybulev P. G., 2015a, The Astronomer's Telegram, 7667, 1
Trushkin S. A., Nizhelskij N. A., Tsybulev P. G., 2015b, The Astronomer's Telegram, 7716, 1
Tsubono K., Aoki T., Asuma K., Daishido T., Kida S., Nakajima H., Niinuma K., Takefuji K., 2015, The Astronomer's Telegram, 7701, 1
Vadawale S. V., Rao A. R., Nandi A., Chakrabarti S. K., 2001, A&A, 370, L17
Varniere P., Tagger M., 2002, A&A, 394, 329
Vasilopoulos G., Petropoulou M., 2016, MNRAS, 455, 4426
Wilms J., Allen A., McCray R., 2000, ApJ, 542, 914
Younes G., 2015, GRB Coordinates Network, 17932
in 't Zand J. J. M., Pan H. C., Bleeker J. A. M., Skinner G. K., Gil'Fanov M. R., Siuniaev R. A., 1992, A&A, 266, 283

This paper has been typeset from a TEX/LATEX file prepared by the author.

Table 1. Log of SWIFT XRT and BAT observations considered for analysis

Observation ID	Date	Time	MJD	Exposure time (in sec)	
				XRT	BAT
00643949000	2015-06-15	18:35:08	57188.77	-	1202.12
00031403038	2015-06-18	00:23:00	57191.01	610.5	-
00644520000	2015-06-18	00:45:29	57191.03	216.7	1202.05
00644627000	2015-06-18	13:10:23	57191.54	2303	1202.06
00031403042	2015-06-19	03:48:50	57192.15	1262	-
00645176000	2015-06-20	13:24:38	57193.55	-	542.11
00031403046	2015-06-21	14:30:58	57194.60	240	6.85
00031403045	2015-06-22	02:08:12	57195.08	930.3	-
00031403049	2015-06-22	08:32:24	57195.35	2976.6	-
00031403047	2015-06-22	09:59:31	57195.41	1902.9	-
00033832001	2015-06-23	08:04:12	57196.33	1867.3	8.16
00031403052	2015-06-23	21:27:34	57196.89	275.05	-
00031403054	2015-06-24	05:01:51	57197.20	-	4.6
00033832002	2015-06-24	11:16:25	57197.46	1519.5	-
00031403055	2015-06-25	00:05:45	57198.00	1028.5	-
00031403056	2015-06-25	00:23:15	57198.01	818.5	713.2
00031403057	2015-06-25	03:41:26	57198.15	-	745.6
00031403058	2015-06-25	22:17:00	57198.92	1312.4	-
00033861001	2015-06-26	12:37:36	57199.52	1482.7	703.4
00031403060	2015-06-26	23:49:54	57199.99	1417.9	1233.0
00033861002	2015-06-27	09:23:56	57200.39	1472.1	-
00031403062	2015-06-27	22:10:25	57200.92	1574.4	-
00031403064	2015-06-28	23:43:58	57201.99	1552.1	-